E3S Web of Conferences **730**, 02008 (2026) https://doi.org/10.1051/e3sconf/202673002008
Soft Soils 2026

Numerical modelling of suction diffusion in unsaturated expansive soils under climatic fluctuations

Mathilde Lefebvre [1,2*], *Mathilde* Morvan [1], *Alaa* Chateauneuf [1,2], and *Nadim* Abdelnour [2]

[1] Université Clermont Auvergne, Clermont Auvergne INP, CNRS, Institut Pascal, Clermont-Ferrand, France
[2] CIDECO, 28 Place Henri Dunant, TSA 50400, F-63001 Clermont-Ferrand Cedex 1, France

Abstract. The behaviour of expansive clay soils is highly influenced by climatic variations that govern the hydric exchanges between the atmosphere and the ground surface. These fluctuations cause changes in soil suction, leading to significant volumetric variations in expansive soils and resulting in differential settlements of lightweight structures, which can induce structural damage. Despite the critical role of these hydroclimatic processes, few models are able to describe the evolution of soil suction under realistic boundary conditions. In this study, a two-dimensional diffusion model is proposed to simulate the temporal and spatial evolution of suction beneath a structure, considered as impermeable, under the influence of climatic fluctuations and over selected time steps. The model is based on the numerical solution of the diffusion equation in unsaturated porous medium, formulated in terms of suction. The boundary conditions incorporate a surface water balance accounting for infiltration and evaporation, using meteorological data from the Météo-France SIM2 model. Hydraulic soil parameters, such as unsaturated permeability and water retention curve expressing suction as a function of water content, are defined from empirical relationships reported in the literature. The model is applied to a clay soil whose parameters are derived from the Chaingy experimental site (France) using daily climatic data for the year 2025. The simulations highlight a strong seasonal variability of suction concentrated within the upper soil layers, while the presence of an impermeable surface zone representing the structure significantly attenuates suction fluctuations beneath the foundation and induces marked horizontal gradients during dry periods.

1 Introduction

France, like many other countries, is highly exposed to the phenomenon of shrinking and swelling of clay soils. The national hazard mapping, updated in January 2026, estimates that 55% of metropolitan territory is subject to medium to high hazard levels, corresponding to nearly 12.1 million individual houses [1].

Drought-related damage has significantly increased since 2017. While it accounted for only 25–35% of total insurance compensations over the 2010–2016 period, it has reached an annual average of 56% since 2017, according to the report published by the Caisse Centrale de Réassurance, the French state-owned reinsurance company [2]. Over the same periods, the average annual cost of drought-induced damage increased from €300 million to €1.1 billion. CCR projections indicate a continued rise in such damage by 2050 [3].

These damages result from hydric variations affecting expansive clay soils. Drought episodes induce an increase in soil suction, leading to volumetric shrinkage that may generate differential settlements beneath shallow foundations. Therefore, a proper understanding of these mechanisms relies on the ability to describe the spatio-temporal evolution of hydric variations within the soil as a function of climatic conditions.

The evolution of the hydric state of near-surface unsaturated soils depends on exchanges at the soil–atmosphere interface, which constitutes a dynamic boundary subjected to alternating fluxes induced by precipitation and evapotranspiration [4]. Several studies have shown that, in fine-grained soils, suction distribution is mainly governed by environmental conditions (infiltration and evapotranspiration) as well as by the hydraulic properties of the material [5–8]. Estimating the hydric regime requires the combined consideration of these parameters.

The modelling of these hydric transfers is mainly based on three types of approaches, depending on the considered state variable:

- Water content–based approaches: although volumetric variations in fine-grained soils are generally associated with suction changes in the literature, some authors consider that analysing variations in water content may be sufficient to predict hydric evolution, particularly due to the relative ease of measuring this variable compared to matric suction [7]. Among these approaches, the works of Briaud et al. [9] and the numerical simulations proposed by Overton et al. [10] can be mentioned.

* Corresponding author: mathilde.lefebvre@cideco.tech

- Suction-based formulations: suction is considered a more relevant variable than water content for representing the hydric state of an unsaturated soil [11]. The diffusion model proposed by Mitchell [12] is one of the most widely used formulations for expansive soils; it has been applied in several recent studies[13–16]. Other developments may also be mentioned, such as the model proposed by Adem and Vanapalli [17].
- Saturated–unsaturated flow analyses (Richards' equation): these models describe transient water flow by incorporating suction-dependent hydraulic conductivity and storage functions [18, 19]. Empirical or semi-empirical formulations were initially proposed to represent infiltration [20, 21] cited in [7]. Extended formulations based on partial differential equations were later developed to model transient flow in unsaturated media [22–26]. The main variables in these models are negative pore-water pressure or hydraulic head.

Although these approaches allow the representation of hydric regime evolution in unsaturated soils, their application to expansive clay soils raises several difficulties. On one hand, hydraulic properties (hydraulic conductivity function and storage function) strongly depend on suction and evolve under the effect of hydric cycles. On the other hand, the realistic definition of boundary conditions at the soil–atmosphere interface constitutes a critical issue, particularly when transient climatic data are introduced.

The present study considers saturated–unsaturated flow modelling. The model is formulated in terms of negative pore-water pressure and relies on the transient solution of the governing equation for flow in unsaturated porous media. The surface boundary conditions are defined as a time-varying water flux obtained from a climatic balance based on meteorological data from the SIM-2 model developed by Météo-France [27, 28].

The aim of this study is to estimate the spatio-temporal evolution of the negative pore-water pressure in expansive clay soil subjected to realistic climatic fluctuations, considering the presence of a shallow structure modelled as an impermeable zone.

2 Model formulation

This section presents the modelling framework used to simulate the transient evolution of moisture conditions in unsaturated soil under climatic action. The problem is formulated in terms of pore-water pressure $U_w(x, y, t)$ (Pa), with matric suction defined as:

$$s(x, y, t) = -U_w(x, y, t), s \geq 0 \tag{1}$$

since the analysed soil layer is located above the groundwater table and therefore remains in an unsaturated state throughout the simulation.

A two-dimensional domain (x, y) is considered. The upper boundary represents the soil–atmosphere interface and is subjected to hydric variation, while a shallow impermeable zone is introduced to represent the structure.

The geometry of the computational domain and the boundary conditions used in the simulations are illustrated in Fig. 1.

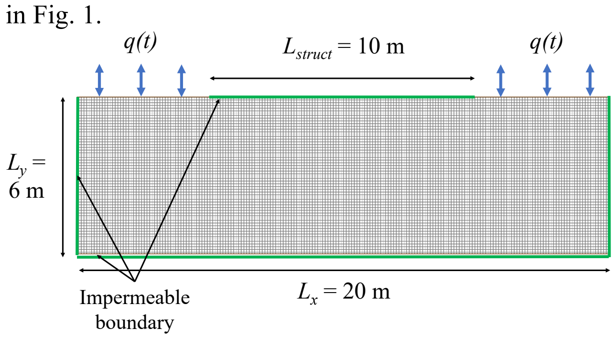

Fig. 1. Geometry of the two-dimensional domain and boundary conditions used in the simulations

2.1 Diffusion model

The governing equation relies on a simplified representation of unsaturated flow, in which the soil is assumed isotropic, gravitational effects are neglected, and air pressure is assumed to dissipate instantaneously.

The transient evolution of pore-water pressure in two dimensions is given by:

$$\frac{\partial U_w}{\partial t} = \frac{\partial}{\partial x}\left(\frac{k_w(s)}{\rho_w\, g\, m_2^w(s)}\left(\frac{\partial U_w}{\partial x}\right)\right) + \frac{\partial}{\partial y}\left(\frac{k_w(s)}{\rho_w\, g\, m_2^w(s)}\left(\frac{\partial U_w}{\partial y}\right)\right) \tag{2}$$

where k_w is the hydraulic conductivity, m_2^w the water storage coefficient (variation of volumetric water content with suction), U_w the pore-water pressure, x and y are the spatial coordinates of the two-dimensional domain ρ_w the water density, and g the gravitational acceleration.

The soil–water retention curve (SWRC) is described using the Fredlund and Xing [29] formulation:

$$\theta(s) = \frac{\theta_s}{\left[\ln\left(e + \left(\frac{s}{a}\right)^n\right)\right]^m} \tag{3}$$

The parameters a, n and m are estimated following the procedure proposed by Zapata [6], based on the percentage passing the No. 200 sieve and the plasticity index.

The storage term is obtained as:

$$m_2^w(s) = -\frac{d\theta}{ds} \tag{4}$$

The unsaturated hydraulic conductivity is derived from the SWRC through numerical integration following Fredlund and Xing approach, based on the Childs and Collis-George approach [30]. Since the in-situ suction values do not exceed residual suction, the correction factor is set equal to one.

The conductivity is expressed as:

$$k_w(s) = k_{sat}\, k_r(s) \tag{5}$$

with:

$$k_r(s) = \int_s^{s_{res}} \frac{\theta(e^y) - \theta(s)}{e^y}\, \theta'(e^y)dy \Bigg/ \int_{s_{aev}}^{s_{res}} \frac{\theta(e^y) - \theta_s}{e^y}\, \theta'(e^y)dy \tag{6}$$

where s_{res} is the residual suction, s_{eav} the air-entry suction, y the integration variable representing suction, θ' the derivative of the retention function with respect to suction (Eq. 3), and θ_s the volumetric water content at saturation.

A lower bound of 10^{-14} m/s is imposed for hydraulic conductivity, corresponding to vapour permeability [31].

The governing equation is nonlinear because both conductivity and storage depend on suction, which depends on the unknown pore-water pressure field. To limit computational cost, hydraulic coefficients are updated using suction values from the previous time step, resulting in a linearised problem at each increment. Given the daily time step adopted here, this approximation is considered acceptable.

The problem is solved using a finite difference scheme.

2.2 Boundary and climatic conditions

The computational domain consists of a rectangular grid of size (N_x, N_y), and the solution is updated at each time step Δt.

2.2.1 Lateral and bottom boundary conditions

The lateral boundaries are assumed sufficiently distant so that horizontal moisture exchanges are negligible. A zero-flux (Neumann) condition is imposed, as following:

Left boundary:

$$U_w(x = 0, y, t) = U_w(x = dx, y, t) \quad (7)$$

Right boundary:

$$U_w(x = L_x, y, t) = U_w(x = L_x - dx, y, t) \quad (8)$$

where L_x is the horizontal length of the domain and dx the spatial discretisation step.

The bottom boundary is also assumed impermeable, leading to:

$$U_w(x, y = L_y, t) = U_w(x, L_y - dy, t) \quad (9)$$

where L_y is the depth of the domain and dy the vertical discretisation step.

2.2.2 Upper boundary condition

The upper boundary represents the soil–atmosphere interface. The foundation is modelled as a central impermeable strip along the ground surface. A zero-flux Neumann condition is therefore imposed in this zone:

$$U_w(x \in foundation, y = 0, t) = U_w(x \in foundation, y = dy, t) \quad (10)$$

Outside the foundation, the bare soil surface is subjected to a vertical water flux calculated from the surface water balance equation. The boundary condition is expressed as:

$$-k_w(s)\frac{\partial Uw}{\partial y} = \rho_w\, g\, q(t) \quad (11)$$

where $q(t)$ is the daily flux, taken as positive for infiltration.

2.2.3 Daily flux

The daily flux $q(t)$ imposed at the soil–atmosphere interface is derived from the SIM2 climatic model developed by Météo-France [27, 28]. It is computed from the surface water balance, which accounts for precipitation, actual evapotranspiration, and surface runoff.

$$q_{SIM2}(t) = P - AE - R \quad (12)$$

where P is the precipitation (rainfall and snowmelt), AE actual evapotranspiration, R surface runoff, and $q_{SIM2}(t)$ the resulting surface flux expressed in mm/day.

Soil permeability controls the effective infiltration and exfiltration capacity at the soil–atmosphere interface. When the imposed atmospheric flux exceeds the hydraulic capacity of the soil, the effective flux is limited by the hydraulic conductivity evaluated at the previous time step.

In such cases, surface ponding is considered: the excess water that cannot infiltrate is temporarily stored at the ground surface and carried over to the next time step. The surface water balance is then updated at each time increment to account for the accumulated volume.

2.3 SIM2 climatic model

The climatic data used in this study are obtained from the SIM2 hydrometeorological system, which couples the SAFRAN, ISBA, and MODCOU models [27, 28]. The system operates on a regular grid of approximately 8 km × 8 km covering metropolitan France. Time series are available from 1958 till now, with daily, 10-day, and monthly outputs.

The SAFRAN module performs a meteorological analysis by combining ground-based observations (notably weather stations) with outputs from numerical weather prediction models. This approach enables the spatial reconstruction of atmospheric variables required for surface water and energy balances, including liquid and solid precipitation, air temperature and humidity, wind speed, and shortwave and longwave radiation.

The ISBA land surface model [32, 33] uses this atmospheric forcing to simulate water and energy exchanges at the soil–vegetation–atmosphere interface. Based on precipitation, radiation, and air thermodynamic conditions, it estimates actual evapotranspiration, surface runoff, drainage and the evolution of soil water storage. Surface characteristics (land cover and vegetation parameters) are derived from the ECOCLIMAP database [34], while soil hydraulic properties are assigned using the Harmonized World Soil Database [35].

The MODCOU module [36] uses the fluxes simulated by ISBA to model surface and subsurface flows at the watershed scale. This component is not directly used in the present study.

In our work, daily variables from the SAFRAN–ISBA chain are used. The grid cell corresponding to the study site is selected based on its geographical coordinates (Lambert II extended projection), retaining the nearest grid point to the site location.

3 Application

The model is applied to an expansive clay whose hydromechanical properties correspond to those of the experimental site instrumented by BRGM in the city of Chaingy (Loiret, France) [37].

3.1 Climatic data

The selected SIM2 data correspond to the data of the nearest node to the experimental site, located at an approximate horizontal distance of 1.9 km. In the Lambert II extended projection, its coordinates are: LAMBX = 5578.8 hm and LAMBY = 23207.2 hm.

Climatic data are extracted over the period from 1st January to 31st December 2025, with a daily time step.

Fig. 2 shows the daily surface flux over the year 2025. Values range from +20 mm/day (intense rainfall events) to −4.3 mm/day (periods dominated by evapotranspiration). The annual mean flux is 0.3 mm/day, with a standard deviation of 3.7 mm/day.

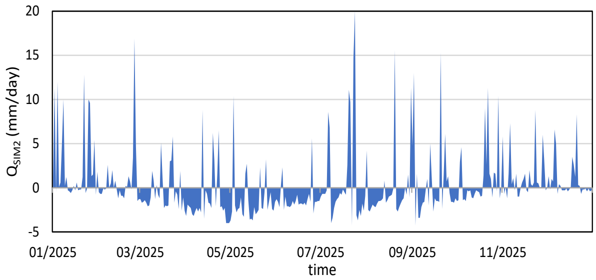

Fig. 2. Daily surface water flux derived from the SIM2 model in Chaingy over 2025.

Fig. 3 presents the cumulative surface flux over the same period. Three main phases can be identified: a recharge phase from January to March, followed by a progressive moisture deficit from April to August, and a renewed recharge phase beginning in September. This seasonal pattern governs the suction gradient simulated within the soil profile.

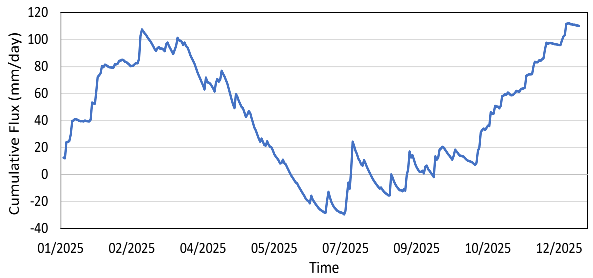

Fig. 3. Cumulative surface water flux in Chaingy over 2025.

3.2 Model geometry and parameters

The domain is modelled as a two-dimensional vertical cross-section. It extends 20 m horizontally and 6 m in depth. Below this layer, investigations indicate the presence of a limestone formation that is considered insensitive to seasonal moisture variations.

The structure is represented by a central impermeable strip 10 m wide at the ground surface. The domain is discretised using 300 nodes in the horizontal direction and 30 nodes in the vertical direction. A daily time step is adopted.

Table 1. Geometrical characteristics and discretisation parameters.

Parameter	Symbol	Value	Unit
Domain horizontal length	L_x	20	m
Domain depth	L_y	6	m
Structure length	L_{struct}	10	m
Number of horizontal nodes	N_x	300	–
Number of vertical nodes	N_y	30	–
Time step	Δt	1	day

3.3 Soil properties and initial conditions

The soil corresponds to a clay or marly clay classified as A3s according to the French GTR classification system. Based on the geotechnical criteria used for national shrink–swell hazard mapping, this material is considered highly susceptible to shrink–swell behaviour [37].

The saturated hydraulic conductivity is set at 10^{-8} m/s, corresponding to a maximum infiltration capacity of approximately 0.9 mm/day.

Table 2. Soil properties used in the simulations

Parameter	Symbol	Value	Unit
Dry unit weight	γ_d	17.5	kPa
Unit weight of solids	γ_s	25.5	kPa
Liquid limit	LL	55	%
Plasticity index	PI	33	%
Percent passing 75 µm	$P_{75\mu m}$	43.7	%
Saturated hydraulic conductivity	k_{sat}	1×10^{-8}	m/s
Air-entry suction	s_{aev}	120	kPa
Initial suction	s_0	100	kPa
Fitting parameter	a	92.0	–
Fitting parameter	n	0.68	–
Fitting parameter	m	1.12	–

The initial condition is taken as a uniform suction field of 100 kPa throughout the entire domain, corresponding to a moist initial state, as the simulation starts in January following a preceding wet period.

The soil-water retention curve used in the simulations, obtained from the Fredlund and Xing formulation with the parameters listed in Table 2, is shown in Fig. 4.

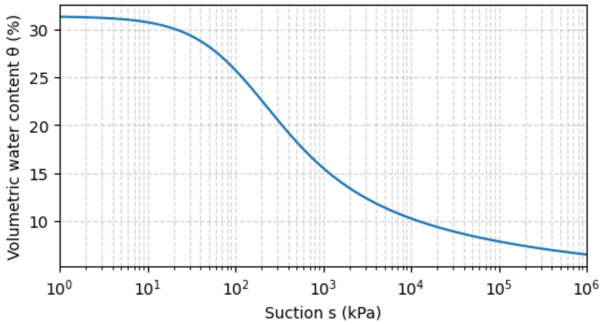

Fig. 4. Soil-water retention curve (SWRC) used in the simulations.

4 Results and discussion

The model calculates the spatio-temporal evolution of the suction field within the soil mass over the entire year 2025, with the volume of water temporarily stored at the surface when infiltration capacity is exceeded (ponding).

The analysis focuses on the extreme hydric states identified during the analysis.

4.1 Spatial variation of soil suction

Three representative dates were selected to characterise the most critical hydric conditions, as shown in Fig. 5:

- 27 February 2025: maximum ponding event, with 58 mm of water accumulated at the uncovered ground surface.
- 15 August 2025: maximum suction reached within the domain, with a surface value of 760 kPa (Fig. 3.).
- 31 December 2025: minimum suction observed during the year, with a maximum value in the soil of approximately 45 kPa. This date coincides with the maximum annual cumulative flux and a ponding volume of 39.9 mm (Fig. 3).

4.1.1 Maximum ponding – 27 February 2025

The 27 February event corresponds to the most significant surface ponding observed during the year, with an accumulation of 58 mm. This reflects a temporary exceedance of the soil infiltration capacity.

4.1.2 Dry state – 15 August 2025

On 15 August, the soil exhibits a pronounced drying state at the uncovered surface. Suction reaches 760 kPa at the bare ground surface, indicating a strong moisture deficit.

Beneath the structure, the absence of direct atmospheric forcing limits the increase in suction. A marked horizontal gradient develops near the edges of the foundation, with a difference of approximately 330 kPa between the centre and the edges. However, this drying effect is mainly confined to the first 0.6–0.7 m beneath the surface, while the soil remains less affected by seasonal variations at greater depth.

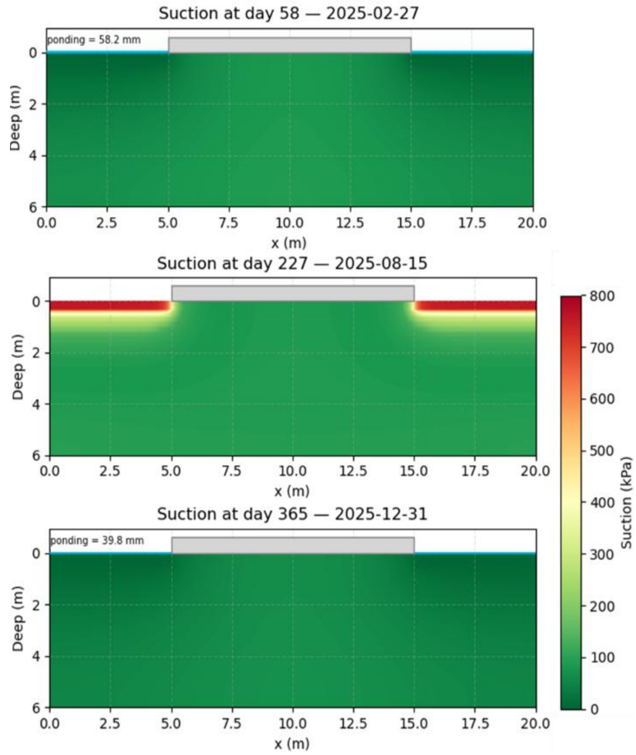

Fig. 5. Spatial distribution of suction for the three representative hydric states in 2025.

4.1.3 Wet state – 31 December 2025

At the end of the year, the soil profile is significantly rehumidified. The maximum suction within the domain is on the order of 45 kPa, indicating conditions close to saturation.

The results also show that dry zones may persist at depth for several weeks following intense rainfall events. For example, during the 26 June 2025 episode, despite surface ponding, only a thin superficial layer exhibits a significant suction reduction, while the underlying soil mass remains desiccated (Fig. 6).

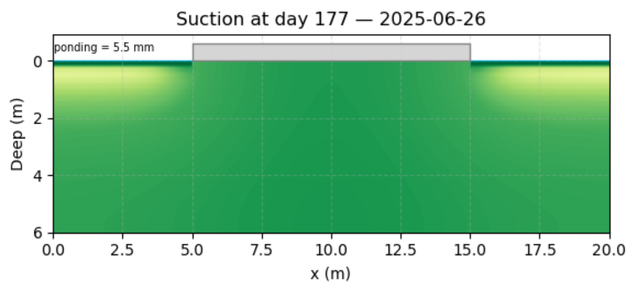

Fig. 6. Limited downward propagation of the wetting front during the 26 June 2025 event.

4.2 Annual suction envelopes for 2025

Annual suction envelopes, defined as the minimum and maximum values reached at each depth over the year 2025, are presented in Fig. 7 for two locations: beneath the centre of the foundation and at a bare soil surface away from the structure. The corresponding annual mean suction profiles are also shown.

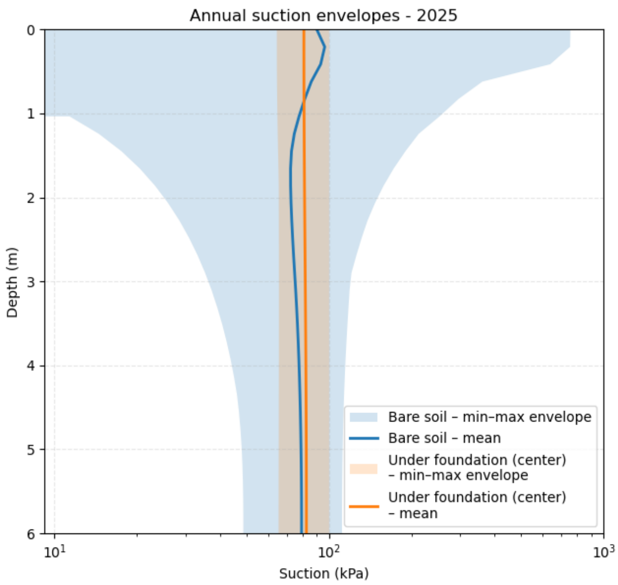

Fig. 7. Annual suction envelopes (minimum, maximum, and mean profiles) beneath the foundation and at the bare surface for 2025.

At the bare surface location, the minimum annual suction values indicate that the soil reaches saturated conditions over the first meter of depth, while minimum suction remains close to 50 kPa below this depth. In contrast, the maximum envelope shows that the largest seasonal fluctuations are concentrated within the upper 0.6 m, where suction ranges from 0 to 760 kPa. Annual variations remain moderate over the next 2 m, generally within the range of 0–250 kPa, and become minor at greater depths, where suction stabilises between approximately 50 and 110 kPa.

Beneath the centre of the foundation, the annual amplitudes are significantly reduced and more uniform over the full depth of the clay layer. Suction varies approximately between 60 and 100 kPa throughout the year, reflecting a buffering effect associated with the absence of direct surface flux.

The computed annual mean suction is 79 kPa beneath the foundation and 82 kPa in the uncovered zone. Despite strongly different seasonal amplitudes, the mean values remain close.

4.3 Discussion

The results highlight a pronounced attenuation of suction variations beneath the structure compared to exposed areas. However, the reduced amplitude observed under the foundation is directly influenced by the modelling assumptions, particularly the prescribed initial suction. In addition, the present configuration represents a simplified theoretical case in which the foundation is located directly at the ground surface. In practice, shallow foundations are generally embedded below the ground level, which would modify the distribution of suction.

In a one-year transient simulation, the initial hydric state may significantly affect the computed annual mean suction beneath the structure. Extending the analysis over a longer period, or adopting an initial condition obtained from a multi-year preliminary simulation, would reduce this dependency and provide a more representative long-term response.

The treatment of ponding also represents a sensitive aspect of the model. The maximum simulated accumulation (58 mm), under a unit hydraulic gradient and with the adopted permeability value, corresponds to a theoretical infiltration time exceeding 60 days. This mechanism may artificially prolong recharge phases in the simulation. A lower hydraulic conductivity would further amplify this effect by increasing the volume of water temporarily stored at the surface and slowing the downward propagation of the wetting front.

Finally, the assumption of a homogeneous soil profile constitutes a simplification. Field observations indicate the presence of distinct clayey facies, which may introduce contrasts in hydraulic conductivity and modify the vertical propagation of moisture variations.

5 Conclusion

This study presents a two-dimensional numerical model for simulating the spatio-temporal evolution of suction in expansive clay subjected to realistic climatic conditions. The application to the clay soil considered in this study shows that seasonal variations are mainly confined to the upper 0.6 m of the soil profile. The presence of a surface impermeable zone representing the structure induces a significant buffering effect beneath the foundation and generates pronounced horizontal suction gradients during dry periods.

The results emphasise the key role of soil hydraulic properties in controlling rehumidification dynamics and the amplitude of seasonal suction fluctuations. They also confirm the necessity of explicitly representing atmospheric boundary conditions in order to capture both desiccation and recharge mechanisms.

Several developments could further enhance the realism of the model:

- introducing a stratified soil profile including topsoil and underlying marly horizons to extend the analysis beyond the active depth;
- accounting for hydraulic anisotropy and localised non-uniform forcing (e.g. vegetation effects or accidental water inputs);
- performing a parametric analysis to investigate the influence of key parameters such as foundation width and saturated hydraulic conductivity on suction distribution;
- comparing the simulations with in-situ water content measurements, potentially combined with an inverse identification procedure for hydraulic parameters.

These perspectives contribute to the development of an integrated soil–atmosphere–structure framework capable of quantifying the impact of climatic fluctuations on structures founded on shrink–swell susceptible clay soils.

References

1. Ouvrard A-E, Bourillet C (2026) Arrêté du 9 janvier 2026 modifiant l'arrêté du 22 juillet 2020 définissant les zones exposées au phénomène de mouvement de terrain différentiel consécutif à la sécheresse et à la réhydratation des sols argileux - Légifrance.
2. Moncoulon D, Desarthe J, Naulin JP, et al (2023) Conséquences du changement climatique sur le coût des catastrophes naturelles en France à l'horizon 2050. Caisse Centrale de Réassurance & Météo France, Paris https://www.ccr.fr/wp-content/uploads/2025/07/Etude-Climatique-2018-version-complete.pdf
3. France Assureurs (2021) Impact du changement climatique sur l'assurance à l'horizon 2050. https://www.franceassureurs.fr/wp-content/uploads/2022/09/vf_france-assureurs_impact-du-changement-climatique-2050.pdf
4. Fredlund DG (2012) Unsaturated Soil Mechanics in Engineering Practice. https://doi.org/10.1061/(asce)1090-0241(2006)132:3(286)
5. Fredlund DG, Rahardjo H (1993) An overview of unsaturated soil behaviour. Geot. special pub. 1–1
6. Zapata CE (1999) Uncertainty in soil-water-characteristic curve and impacts on unsaturated shear strength predictions. Arizona State University
7. Bulut R, Javid AH (2019) Developing Implementable Climatic Input Data and Moisture Boundary Conditions for Pavement Analysis and Design
8. Javid AH, Bulut R (2022) A Mechanistic-Empirical Model to Predict Suction Profile in Subgrade Soil. Tran-SET 2020,87–99 https://doi.org/10.1061/9780784483305.009
9. Briaud J-L, Zhang X, Moon S (2003) Shrink Test-Water Content Method for Shrink and Swell Predictions. J. Geotech. Geoenviron. Eng. **129**,590–600. https://doi.org/10.1061/(ASCE)1090-0241(2003)129:7(590)
10. Overton DD, Chao K-C, Nelson JD (2006) Time rate of heave prediction for expansive soils. In: GeoCongress 2006, 1–6 https://doi.org/10.1061/40803(187)162
11. Richards LA (1931) Capillary conduction of liquids through porous mediums. Physics 1,318–333 https://doi.org/10.1063/1.1745010
12. Mitchell PW (1980) The structural analysis of footings on expansive soil. In: Expansive soils. ASCE, p. 438
13. Cai S, Saha S, Birgisson B, Lytton R (2025) Development of a mechanistic-empirical framework to predict moisture variation for clayey subgrade soil. Int. J. Pavement Eng. **26** https://doi.org/10.1080/10298436.2025.2485309
14. Javid AH, Bulut R (2023) Equilibrium Suction Prediction Model for Subgrade Soils in Oklahoma. Int. J. Geomech. **23**. https://doi.org/10.1061/IJGNAI.GMENG-7076
15. Saha S, Hariharan N, Gu F, et al (2019) Development of a mechanistic-empirical model to predict equilibrium suction for subgrade soil. J. Hydrol. **575**,221–233. https://doi.org/10.1016/j.jhydrol.2019.05.035
16. Yue Chen, Yue Chen, Yue Chen, et al (2022) Analysis of the Depth of the Active Zone via Coupled Hydro-Mechanical Analysis. Geo-Congress 2022. https://doi.org/10.1061/9780784484050.035
17. Adem HH, Vanapalli SK (2014) Elasticity moduli of expansive soils from dimensional analysis. Geotech. Res. **1**:60–72. https://doi.org/10.1680/gr.14.00006
18. Cherry JA, Freeze RA (1979) Groundwater. Englewood Cliffs, NJ: Prentice-Hall
19. Gitirana G, Fredlund M (2005) Infiltration-runoff boundary conditions in seepage analysis. Prof the 58th Can. Geotech. Conf., Saskatoon, Canada, 18-21 September
20. Horton (1933) The Rôle of infiltration in the hydrologic cycle. Eos Trans AGU **14**:446–460. https://doi.org/10.1029/TR014i001p00446
21. Kostiakov AN (1932) On the dynamics of the coefficient of water percolation in soils and the necessity of studying it from the dynamic point of view for the purposes of amelioration, Transactions of 6th Com. Int. Soc.y of Soil Sci.
22. Vu HQ, Fredlund DG (2004) The prediction of one-, two-, and three-dimensional heave in expansive soils, Can. Geotech. J **41**,713–737. https://doi.org/10.1139/t04-023
23. Abed A (2008) Numerical Modeling of Expansive Soil Behavior
24. Teodosio B, Baduge KSK, Mendis P (2020) Simulating reactive soil and substructure interaction using a simplified hydro-mechanical finite element model dependent on soil saturation, suction and moisture-swelling relationship. Comp. and Geotech. **119**, 103359 https://doi.org/10.1016/j.compgeo.2019.103359
25. Assadollahi H, Nowamooz H (2020) Long-term analysis of the shrinkage and swelling of clayey soils in a climate change context by numerical modelling and field monitoring. Comp. and Geotech. **127**, 103763 https://doi.org/10.1016/j.compgeo.2020.103763
26. Zhang J, Little DN, Hariharan N, Kim Y-R (2019) Prediction of climate specific vertical movement of pavements with expansive soils based on long-term 2D numerical simulation of rainwater infiltration. Comp. and Geotech. **115**, 103172. https://doi.org/10.1016/j.compgeo.2019.103172
27. Habets F (1998) Modélisation du cycle continental de l'eaua l'échelle régionale: application aux bassins versants de l'Adour et du Rhône. PhD Thesis, PhD thesis, Université Paul Sabatier, Toulouse, France

28. Le Moigne P, Besson F, Martin E, et al (2020) The latest improvements with SURFEX v8.0 of the Safran–Isba–Modcou hydrometeorological model for France. Geos. Mod. Dev. **13**, 3925–3946. https://doi.org/10.5194/gmd-13-3925-2020

29. Fredlund DG, Xing A (1994) Equations for the soil-water characteristic curve. Can Geotech J **31**, 521–532. https://doi.org/10.1139/t94-061

30. Childs EC, Collis-George N (1950) The control of soil water. Adv. in agr. **2**:233–272 https://doi.org/10.1016/S0065-2113(08)60766-X

31. Ebrahimi-Birang N, Gitirana Jr GFN, Fredlund DG, et al (2004) A lower limit for the water permeability coefficient. In: Proc. of the 57th Can. Geotech.Conf., Quebec City, 24–27

32. Noilhan J, Planton S (1989) A simple parameterization of land surface processes for meteorological models. Monthly weather review **117**,536–549 https://doi.org/10.1175/1520-0493(1989)117<0536:aspols>2.0.co;2

33. Noilhan J, Mahfouf J-F (1996) The ISBA land surface parameterisation scheme. Glob. and plan. Chang. **13**, 145–159 https://doi.org/10.1016/0921-8181(95)00043-7

34. Faroux S, Kaptué Tchuenté AT, Roujean J-L, et al (2013) ECOCLIMAP-II/Europe: A twofold database of ecosystems and surface parameters at 1 km resolution based on satellite information for use in land surface, meteorological and climate models. Geos. Mod. Dev. **6**, 563–582 https://doi.org/10.5194/gmd-6-563-2013

35. Nachtergaele F, Van Velthuizen H, Verelst L, et al (2010) Harmonized world soil database. In: Proc.of the 19th w. cong. of soil sci., Brisbane, Australia. International Union of Soil Sciences, pp 34–37

36. Ledoux E, Girard G, Marsily G, et al (1989) Spatially Distributed Modeling: Conceptual Approach, Coupling Surface Water And Groundwater. Unsat. Flow in Hyd. Mod., 435–454 https://doi.org/10.1007/978-94-009-2352-2_16

37. Gourdier S (2018) Suivi du site instrumenté « argiles » de Chaingy (Loiret) – Phase 4 : suivi annuel 2017. Programme de travail BRGM-DGPR 2017.Action C.8. BRGM / RP-67802-FR. 44 p.